SANDIA REPORT
SAND2004-1158
Unlimited Release
Printed March 2004

MEMS in Microfluidic Channels

Thomas L. Sounart, Carolyn M. Matzke, Murat Okandan, Carol L. Ashby, and Terry A. Michalske

Prepared by
Sandia National Laboratories
Albuquerque, New Mexico 87185 and Livermore, California 94550

Sandia is a multiprogram laboratory operated by Sandia Corporation,
a Lockheed Martin Company, for the United States Department of Energy's
National Nuclear Security Administration under Contract DE-AC04-94AL85000.

Approved for public release; further dissemination unlimited.

Issued by Sandia National Laboratories, operated for the United States Department of Energy by Sandia Corporation.

NOTICE: This report was prepared as an account of work sponsored by an agency of the United States Government. Neither the United States Government, nor any agency thereof, nor any of their employees, nor any of their contractors, subcontractors, or their employees, make any warranty, express or implied, or assume any legal liability or responsibility for the accuracy, completeness, or usefulness of any information, apparatus, product, or process disclosed, or represent that its use would not infringe privately owned rights. Reference herein to any specific commercial product, process, or service by trade name, trademark, manufacturer, or otherwise, does not necessarily constitute or imply its endorsement, recommendation, or favoring by the United States Government, any agency thereof, or any of their contractors or subcontractors. The views and opinions expressed herein do not necessarily state or reflect those of the United States Government, any agency thereof, or any of their contractors.

Printed in the United States of America. This report has been reproduced directly from the best available copy.

Available to DOE and DOE contractors from
U.S. Department of Energy
Office of Scientific and Technical Information
P.O. Box 62
Oak Ridge, TN 37831

Telephone: (865)576-8401
Facsimile: (865)576-5728
E-Mail: reports@adonis.osti.gov
Online ordering: http://www.doe.gov/bridge

Available to the public from
U.S. Department of Commerce
National Technical Information Service
5285 Port Royal Rd
Springfield, VA 22161

Telephone: (800)553-6847
Facsimile: (703)605-6900
E-Mail: orders@ntis.fedworld.gov
Online order: http://www.ntis.gov/help/ordermethods.asp?loc=7-4-0#online

SAND 2004-1158
Unlimited Release
Printed March 2004

MEMS in Microfluidic Channels

T.L. Sounart
Chemical Synthesis and Nanomaterials

C.M. Matzke
Biomolecular Materials and Interfaces

M. Okandan
MEMS and Novel Silicon Technologies

C.L. Ashby
Intellectual Property Center

T.A. Michalske
Center for Integrated Nanotechnologies

Sandia National Laboratories
P.O. Box 5800
Albuquerque, NM 87185-1413

ABSTRACT

Microelectromechanical systems (MEMS) comprise a new class of devices that include various forms of sensors and actuators. Recent studies have shown that microscale cantilever structures are able to detect a wide range of chemicals, biomolecules or even single bacterial cells. In this approach, cantilever deflection replaces optical fluorescence detection thereby eliminating complex chemical tagging steps that are difficult to achieve with chip-based architectures. A key challenge to utilizing this new detection scheme is the incorporation of functionalized MEMS structures within complex microfluidic channel architectures. The ability to accomplish this integration is currently limited by the processing approaches used to seal lids on pre-etched microfluidic channels. This report describes Sandia's first construction of MEMS instrumented microfluidic chips, which were fabricated by combining our leading capabilities in MEMS processing with our low-temperature photolithographic method for fabricating microfluidic channels. We have explored in-situ cantilevers and other similar passive MEMS devices as a new approach to directly sense fluid transport, and have successfully monitored local flow rates and viscosities within microfluidic channels. Actuated MEMS structures have also been incorporated into microfluidic channels, and the electrical requirements for actuation in liquids have been quantified with an elegant theory. Electrostatic actuation in water has been accomplished, and a novel technique for monitoring local electrical conductivities has been invented.

ACKNOWLEDGEMENTS

Sandia is a multiprogram laboratory operated by Sandia Corp., a Lockheed-Martin Company, for the U.S. Department of Energy under Contract No. DE-AC04-94AL85000. The authors thank Mani Seethambal of the MEMS and Novel Silicon Technologies Department and Peggy Clews of MDL Operations for fabrication support, and George Bachand of the Biomolecular Materials and Interfaces Department for help with biochemical functionalization. We also thank David Czaplewski of the Nanostructure and Semiconductor Physics Department, and Grant Meyer and Harold Craighead at Cornell University for their collaboration on design, fabrication, and testing of integrated microfluidic flow sensors.

Contents

1 Introduction 7

2 Background 7

2.1 Chemical Sensing with Cantilevers 7
2.2 Microfluidic Flow Sensing 7

3 Actuated & Functionalized Cantilevers 10

3.1 Fabrication 10
3.1.1 MEMS cantilevers 11
3.1.2 Functionalization 12
3.1.3 Trilayer film channels 17
3.1.4 Releasing and drying 21
3.1.5 Interconnects 22
3.1.6 Experimental 24

4 Passive Cantilevers in Si/Glass Channels 25

4.1 Cornell Wafers 25
4.2 Sandia MDL Wafers 25

5 Electrostatic Actuation in Liquids 28

6 Conductivity Sensor 30

7 Hydrodynamic Damping Reduction 30

8 Concluding Remarks 30

List of Figures

1 General fabrication process flow. 10
2 Photomicrographs of sample first generation microcantilevers 11
3 Photomicrographs of second generations microcantilevers 13
4 Photomicrographs of sample second generation microcantilevers in channels . 14
5 SEM of electrical connections to cantilevers 15
6 Interferometric characterization of microcantilevers 16
7 Photomicrographs of sample gold-patterned microcantilevers 18
8 Scanning electron micrograph of trilayer SiO_xN_y film channel. 19
9 Scanning electron micrograph of trilayer film with and without pinch-off. . . 20
10 SEM of cone-shaped defects 21
11 Photomicrograph of microfluidic channel interconnect. 23
12 Schematic of the optical deflection measurement system 24
13 SEM of micromechanical plate flow sensor 26
14 Response of the micromechanical plate 27

15 Critical electrostatic actuation frequency 29

1 Introduction

The microfabrication techniques developed by the semiconductor industry to mass produce integrated circuits have more recently been applied to the development of microscale mechanical devices called microelectromechanical systems (MEMS) [1, 2]. Because of their small size and the cost effectiveness of microfabrication, MEMS have the potential to revolutionize many technologies of interest to Sandia, including weapons components, optics, and sensors and actuators of all types. To realize this potential for chemical and biological detection, MEMS devices must operate in a liquid environment and be incorporated into microfluidic channels, which introduces new challenges for device design and fabrication.

This report describes Sandia's first integration of MEMS into microfluidic channels. Two types of integrated sensors were explored—chemically functionalized cantilevers for biomolecular detection, and in-situ flow sensors using cantilever and other related architectures. We begin with some background and theory on cantilever-based chemical detection and microfluidic flow sensing. We then discuss our development of integrated, active MEMS cantilevers, which were constructed using the Microelectronics Development Laboratory's (MDL's) leading 5-level polysilicon surface micromachining process [2], and integrated into SiO_xN_y thin film microchannels [3] fabricated at Sandia's Compound Semiconductor Research Laboratory (CSRL). This will lead to a description of passive cantilever and other similar structures that were fabricated and tested in glass channels at Cornell University, followed by a discussion of our work on electrostatic actuation of silicon MEMS in liquids. We will then close with some concluding remarks.

2 Background

2.1 Chemical Sensing with Cantilevers

Recent studies have shown that microscale cantilever structures are able to detect a wide range of chemicals, biomolecules (nucleic acids and proteins) or even single bacterial cells [4]–[12]. In this approach, cantilever deflection replaces optical fluorescence detection thereby eliminating complex chemical tagging steps that are difficult to achieve with chip-based architectures. In most of the demonstrations, the transduction mechanism has involved a measurement of static cantilever deflection resulting from a change in surface energy when molecules are chemically adsorbed to a functionalized cantilever [4]–[9]. Another sensing method employs the cantilever as a microbalance—the cantilever is actuated dynamically and the adsorbed species are detected by a resonance frequency shift [10]–[12]. Demonstrations and theory of these detection mechanisms are well documented in the literature, but integration of such devices in microfluidic channels has not been reported.

2.2 Microfluidic Flow Sensing

Although commercial microfluidic systems are now available, none include in-situ local flow sensors embedded within the channel networks. Yet, integrated local flow and pressure sensors will be critical for failure analysis, and generally to monitor microfluidic device performance. Development of MEMS-based pressure sensors began in 1983 [13], and they

have been used primarily to measure turbulence [14]. Essentially all microfabricated pressure sensors consist of a thin diaphragm (usually silicon) that is deflected under pressure. The deflection is sensed piezoelectrically, piezoresistively, capacitively, or optically. To date, these sensors have all been fabricated as a separate microchip device that is embedded in a macroscale flow channel such as a wind tunnel.

While there are many transduction mechanisms for sensing flow, microflow sensor development has been concentrated on thermal and mechanical sensors. Thermal micromachined flow sensors (anemometers) have received by far the most attention both in the research literature and with commercial development [18, 19]. The first micromachined thermal flow sensor was presented in 1974 [20], and commercial development began at least as early as 1986 by Toyota [21] and Honeywell [22]. As with micropressure sensors, work on these sensors has been focused on monitoring flows external to the sensor, but several devices integrated into microfluidic channels have been developed [23]–[27]. The sensing principle of all thermal flowmeters involves measuring temperatures to extract the heat transfer rate from a heater element, which increases with increasing flow rate. In the simplest design, a thin resistive element is heated with an electric current, and is cooled convectively by fluid motion over the element. The resistance of the element changes with temperature, so as it is cooled by the flow, the resistance change is measured (e.g. by a change in current at constant power). Liu et al. [28] measured shear stresses as low as 0.05 Pa with a silicon resistor of maximum dimension 200 μm. In another anemometer design, temperatures fore and aft of the heater are measured with surface acoustic wave (SAW) devices [29], but these have a larger footprint.

Development on MEMS mechanical flow sensors began in 1988 with Schmidt et al. [15], and the best sensitivity has been demonstrated by Padmanabhan et al. [16]. Their device, which is essentially a thin plate tethered by 4 beams attached to each corner, measured shear stresses from less than 0.01 Pa up to 10 Pa. However, the Padmanabhan device is not integrated into a microfluidic channel and is 1.5 mm in width; it will lose orders of magnitude sensitivity from scaling it down to fit in the $O(100\ \mu\text{m})$ wide microchannels typical of microfluidic systems. Another microdevice has been reported to measure flow by measuring differential pressure [17]. This type of sensor includes two pressure sensors placed a known distance apart, and the the differential pressure is correlated to the flow rate. Mechanical flow sensor research has been limited to seperate devices that are typically made to be added to a macroscale channel, usually for the purpose of studying turbulence. Mechanical sensors that have already been integrated into a microfluidic channel have not been reported.

Microcantilevers can also be used to directly monitor fluid transport, and are the simplest devices to integrate within microchannels. Although no demonstrations of cantilever flow sensors have been reported, the same transduction mechanisms demonstrated for chemical sensing can be applied toward flow sensing if cantilever structures are integrated into robust microfluidic architectures. A cantilever beam aligned parallel to the flow in a channel will deflect from a differential surface stress $\Delta\sigma$ if the fluid shear stress τ above the beam differs from that below. If the length of the beam l is much longer than the channel depth h, the deflection can be estimated with a one-dimensional theory.

The deflection δ of a beam resulting from a differential surface stress (top surface –

bottom surface) is given by the Stoney equation,

$$\delta = \frac{3\Delta\sigma(1-\nu)l^2}{Et^2}, \tag{1}$$

where ν is Poisson's ratio, E is the Young's Modulus, and t is the thickness of the beam. The interfacial stress σ imposed on the surface of a cantilever beam from fluid shear is given by

$$\sigma(x) = \tau(l-x), \tag{2}$$

where x is the axial position along the cantilever with the origin at the upstream (fixed) end of the beam. For fully developed flow above (subscript 1) and below (subscript 2) the cantilever,

$$\tau_{1,2} = \frac{3\mu v_{1,2}}{h_{1,2}}, \tag{3}$$

where μ and $v_{1,2}$ are the viscosity and average speed of the fluid respectively, and $h_{1,2}$ is the distance between the cantilever and the top or bottom of the channel. Also for fully developed flow, the fluid pressure is cross-sectionally uniform, which requires

$$\frac{v_1}{v_2} = \left(\frac{h_1}{h_2}\right)^2. \tag{4}$$

Combining Eqs. (2)–(4) yields

$$\Delta\sigma(x) = \frac{3\mu v_1}{h_1}(l-x)\left(1-\frac{h_2}{h_1}\right) \tag{5}$$

It is important to note that the Stoney equation (Eq. (1)) assumes a constant differential stress, whereas the stress resulting from fluid shear (Eqs. (2) and (5)) decreases linearly from $\Delta\tau l$ at the upstream end to 0 at the downstream end. However, an upper bound on the deflection $\delta_{\max}$ can be calculated by substituting the maximum $\Delta\sigma$ into Eq. (1), and it can be easily shown that a lower bound is $\geq 3/8 \times \delta_{\max}$. Thus, $\delta_{\max}$ provides a reasonable order of magnitude estimate of the deflection. The upper bound on the deflection, neglecting edge effects, is

$$\delta_{\max} = \frac{9\mu v_1(1-\nu)l^3}{Eh_1t^2}\left(1-\frac{h_2}{h_1}\right). \tag{6}$$

Microfluidic flow speeds typically range up to about 10 cm/s, and h_1 and h_2 are about 20 μm and 2 μm, respectively for the devices fabricated here. So for water flow in our channels, the thinnest cantilevers ($t = 1$ μm) will deflect less than 0.5 nm for 100 μm of length. For optical detection, the deflection should be at least a nanometer, so 100 μm cantilevers will probably not be sensitive enough to measure flow. However, the deflection scales on l^3, so the 200 μm cantilevers might be just at the sensitivity limit for high flow rates, but will likely not provide much dynamic range in flow sensing. Cantilevers with $l \geq 500$ μm are expected to sense at least two orders of magnitude of flow rates in the range typical of microfluidic applications.

3 Actuated & Functionalized Cantilevers

To enable both passive and active cantilever sensing functions, arrays of electrically addressable polysilicon (pSi) cantilevers were fabricated using the Sandia SUMMiT™surface micromachining process [2], and incorporated into our patented trilayer thin film microchannels [3]. The low-temperature photolithographic method of defining microchannels does not destroy sensitive biochemical coatings applied to the cantilevers prior to channel fabrication, and permits sealing the channels across the pSi electrical leads required to actuate the cantilevers embedded in the channels.

3.1 Fabrication

After working with several different fabrication schemes, the final process flow shown in Fig. 1 was developed for producing MEMS cantilever instrumented microfluidic chips. Six

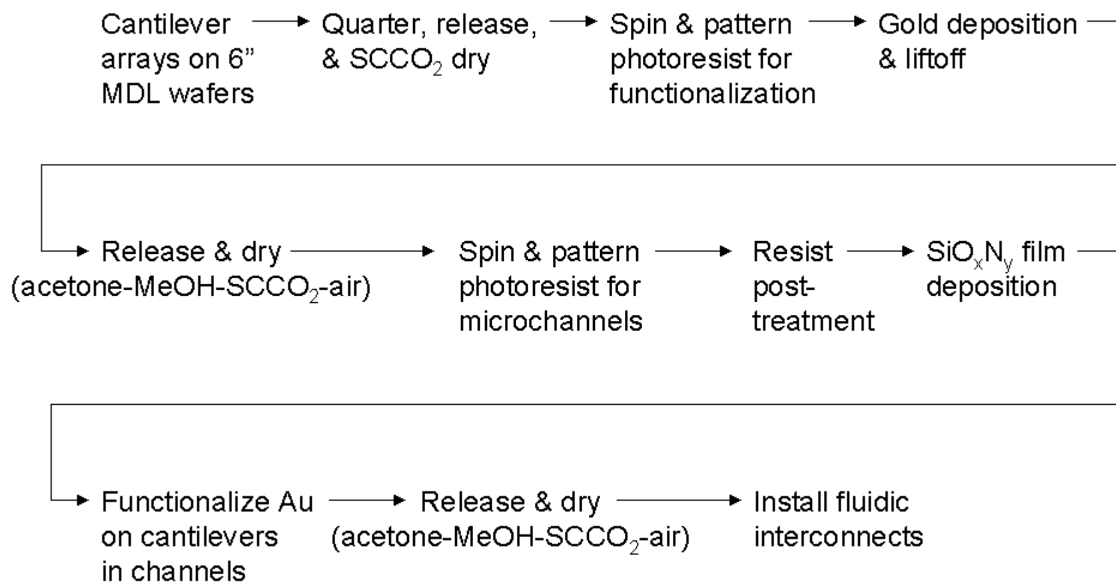

Figure 1: General fabrication process flow.

inch wafers with the cantilever arrays are quartered and released at MDL, and then sent to CSRL for post-processing. Photoresist is spun on the wafer quarters and exposed with a mask patterned for functionalization. A thin layer of gold is deposited and patterned on the cantilevers using a standard liftoff technique. The wafer quarters are then soaked in acetone

to remove resist, transferred to methanol (MeOH), and dried in supercritical CO_2 ($SCCO_2$). Next the wafer is patterned with photoresist using a mask for defining the channels. The resist is reflowed and post-baked, and the SiO_xN_y trilayer film channels are deposited. While encased in photoresist, the wafer quarters are diced into smaller die, and after releasing in acetone and supercritical drying again, capillary interconnections are installed. The chips are then functionalized in-situ with thiol-based direct adhesion to the patterned gold surfaces within the channels. After biomolecular functionalization, the channels can be supercritically dried again or immediately tested for complementary DNA hybridization or protein adsorbtion. The following sections provide details on each component of this fabrication sequence.

3.1.1 MEMS cantilevers

Two generations of MEMS cantilever designs were fabricated at MDL. Sample photographs of the first set of microcantilevers, embedded in the trilayer film channels, are provided in Fig. 2. These passive cantilevers were tested as flow sensors in both SiO_xN_y and poly-

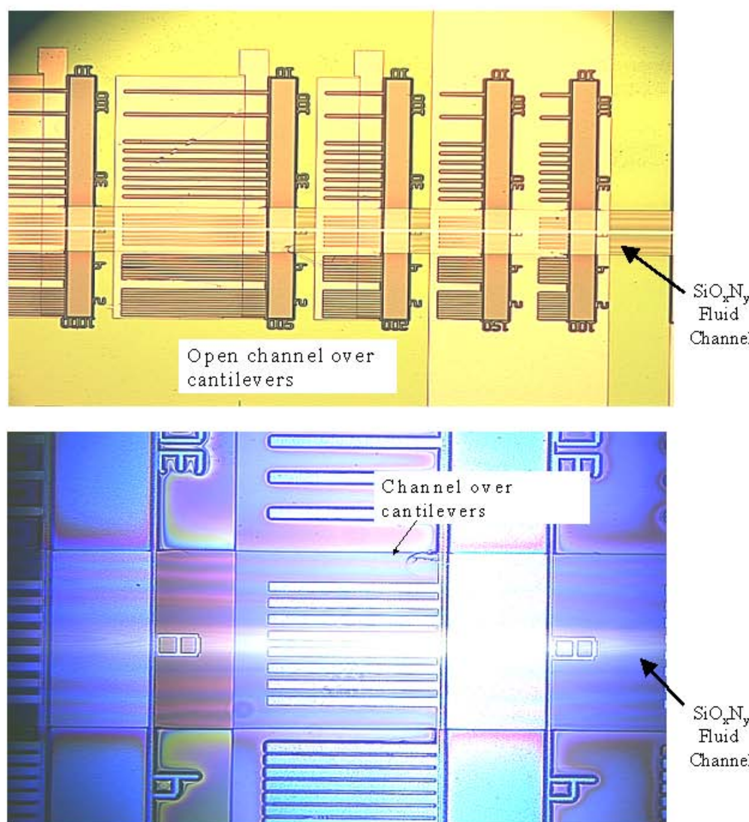

Figure 2: Photomicrographs of sample first generation microcantilevers in SiO_xN_y fluid Channels.

dimethylsiloxane (PDMS) microfluidic architectures, but cantilever deflections were below

the detection limit. However, the base of these cantilever designs included an undercut etch that could not be sealed with the trilayer film, and the integrity of the PDMS microchannel seal was not sufficient to support the pressure-driven flow. So because of leaks, the local flowrate at the cantilevers may have been artificially low.

The second generation microcantilevers (Figs. 3 and 4) were designed to be active sensors, actuated electrostatically. In these devices, electrical connections are wired (pSi) to bond pads for each array of cantilevers, and in some designs, individual cantilevers are electrically addressable (Fig. 5). Also included are cantilever arrays oriented both parallel and perpendicular to the flow direction, and narrow beams with plates on the ends to maximize the surface area on the most sensitive part of the cantilever. Cantilever lengths range from 50 μm to 1 mm, and the designs were fabricated with three different film thicknesses. Three wafers each were produced with 1, 1.5, and 2.5 μm cantilevers, all 2 μm above the first layer of pSi (poly0) deposited on the substrate. Interferometric measurements of released cantilever beams (on test die that are included on all MDL MEMS wafers) show the different shapes and residual stress inherent in each thickness (Fig. 6). The 2.5 μm cantilevers—standard for a composite poly1 and poly2 film—have the lowest residual stress, and are flat to within approximately 1 μm of deflection toward the substrate per 1 mm of length. The 1.5 μm beams deflect away from the substrate with about 3 times the curvature of the 2.5 μm beams, and the 1 μm beam shapes vary substantially with length, including many that deflect away from the substrate at the base, then peak in the middle and deflect back towards the substrate. The design drawings are stored in the MDL library under RD33601A.

3.1.2 Functionalization

Chemical functionalization of the microcantilevers is necessary for their application as chemically selective sensors of the presence of specific biomolecules. In the intially planned process flow, functionalized sensors were to be produced by direct biomolecular adhesion to the pSi cantilevers prior to formation of the microchannels. In comparison to the gold patterning process (Fig. 1), this provides more flexibility with the chemistry, and does not require functionalization within a microchannel—a much less experienced procedure among biochemists. Critical to integration of prefunctionalized sensors in microfluidic channels is a demonstration of the viability of surface-coupled biomolecules against the necessary microfabrication processes, and so tests were performed on Si wafers prior to functionalization of the cantilevers. DNA was selected for the initial studies due to its greater chemical robustness than that of proteins. The first step was to develop a simple and efficient mechanism for adhesion of DNA to compatible surfaces. Three short DNA oligomers were synthesized and labeled with a fluoroscein isothiocyanate dye. This permitted use of epifluorescence microscopy to confirm the presence of DNA following exposure to various microfabrication processes. For adhesion experiments, DNA was diluted in a solution of $MgCl_2$ to provide an overall net positive charge to the DNA. The positive charge on the DNA permits adhesion to SiO_2 but not SiH. To test the compatibility of DNA with microfabrication processing, an oxide layer was thermally grown on a Si wafer. DNA oligomers then were adhered to the SiO_2 surface and tested against the chemical and physical conditions that will be used for processing the cantilevers and microfluidic channels. To ensure that the DNA was bound to the surface and would not be removed by aqueous solutions, the DNA-coated SiO_2 chips were placed

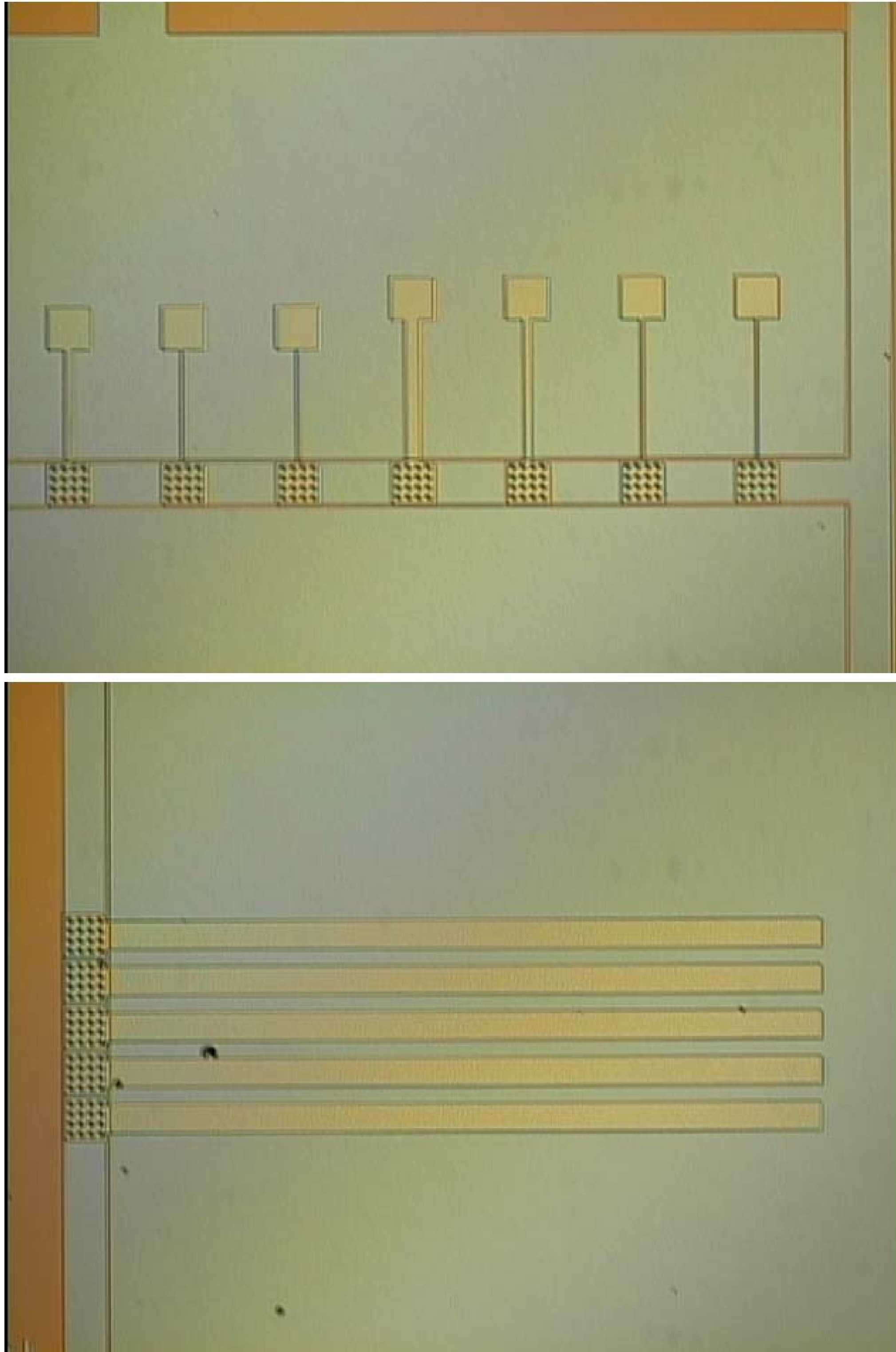

Figure 3: Photomicrographs of selected second generation microcantilevers. In upper photo, cantilever beam lengths range from 80 μm to 100 μm. In lower photo, the beams are 500 μm long and 20 μm wide.

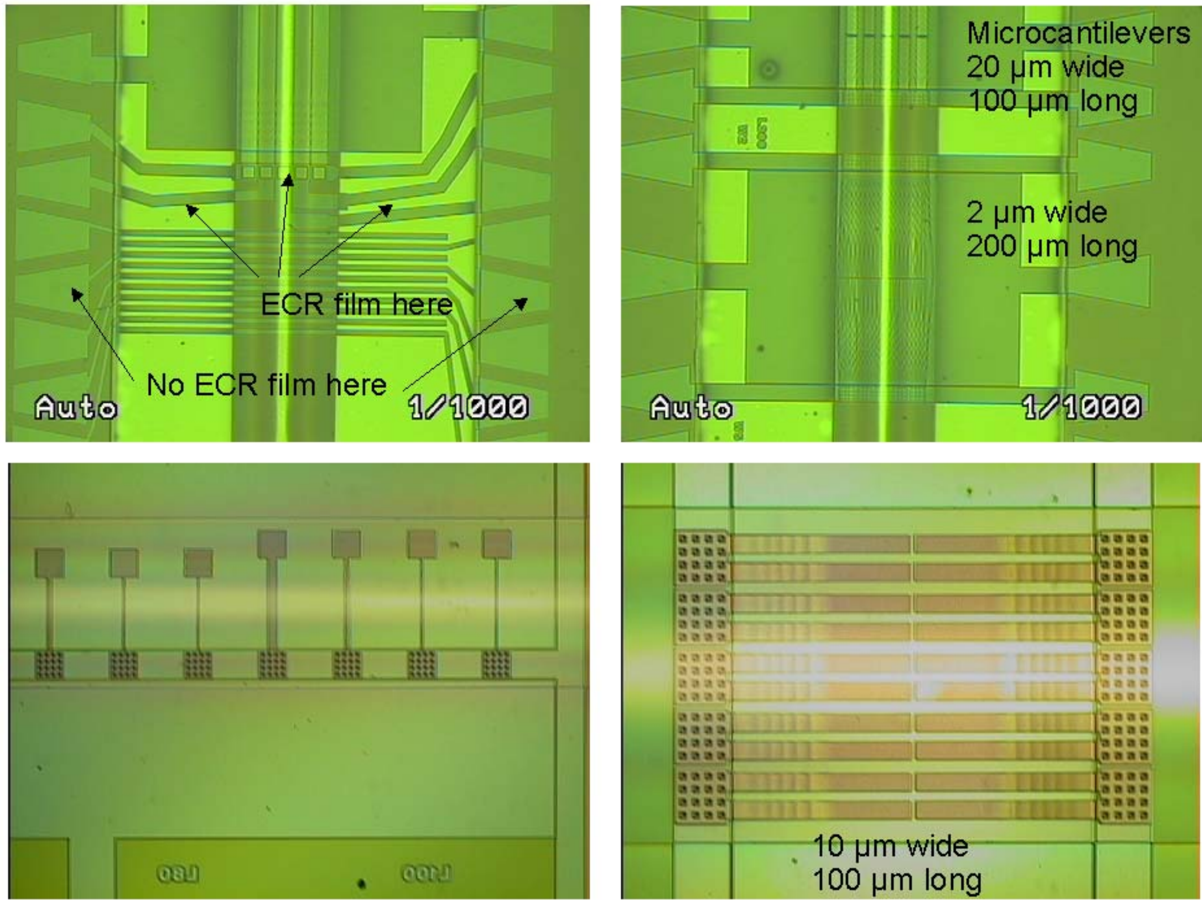

Figure 4: Photomicrographs of sample second generation microcantilevers in SiO_xN_y fluid channels.

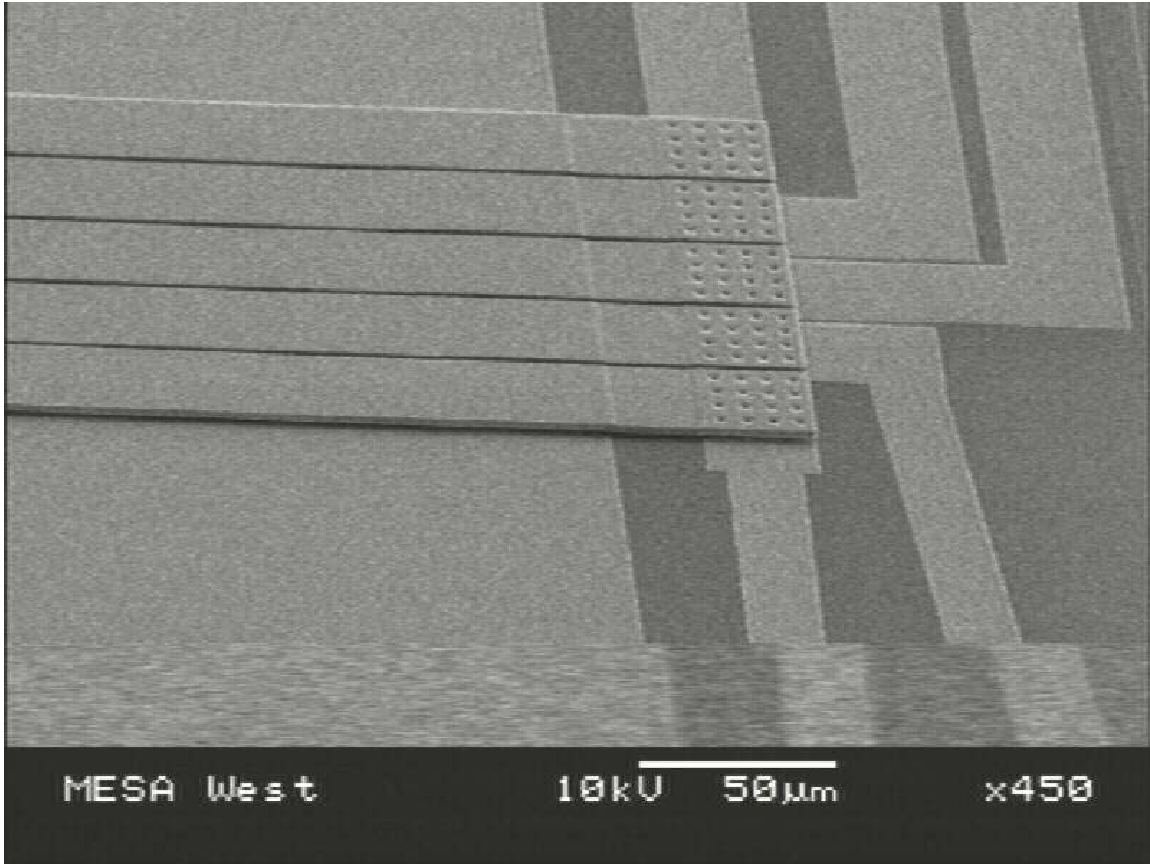

Figure 5: Scanning electron micrograph of pSi electrical connections for individually actuated microcantilevers.

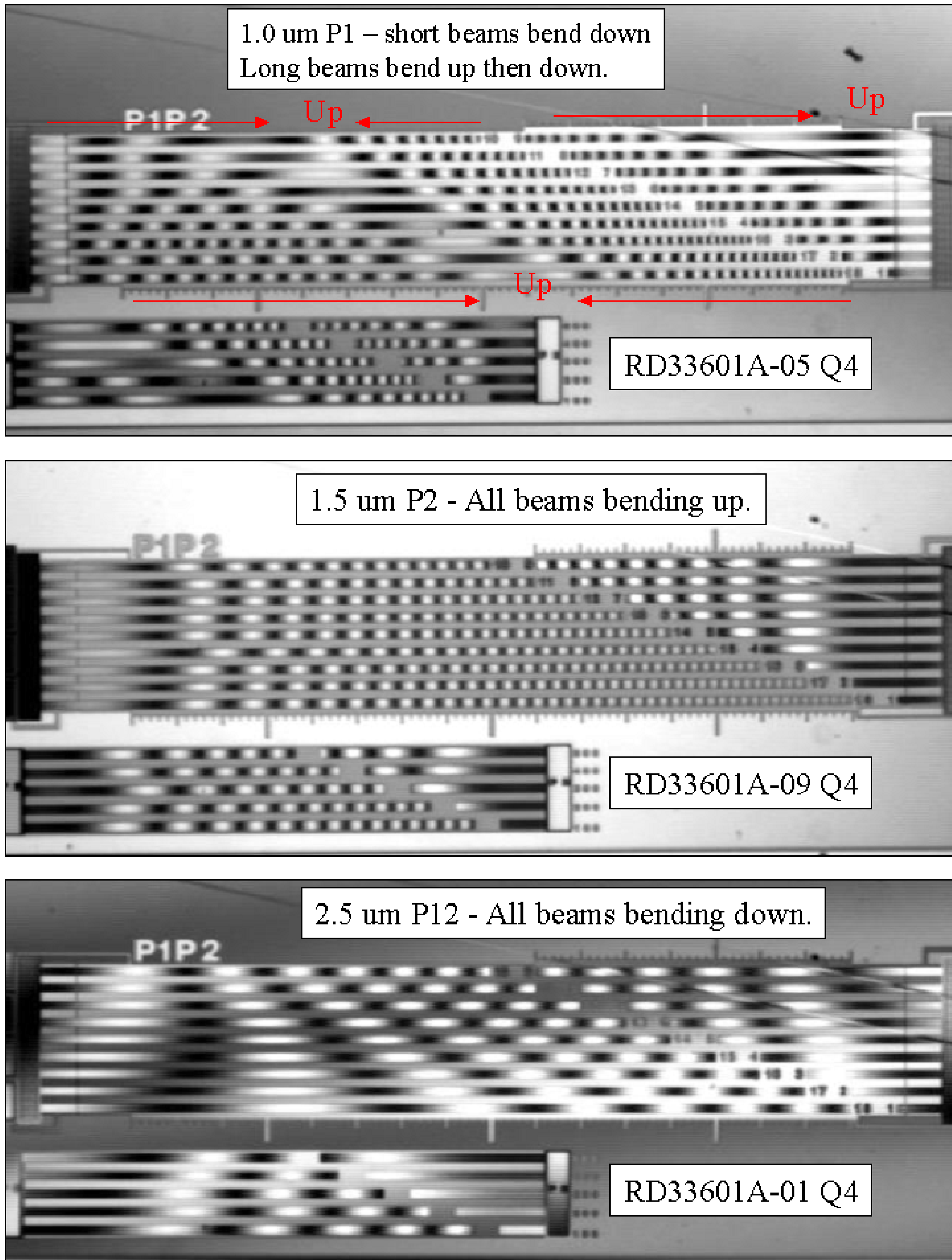

Figure 6: Photomicrographs from interferometric characterization of microcantilevers on test die.

in deionized H_2O overnight at room temperature. The fluorescent signal did not changed following the overnight incubation. The DNA-coated SiO_2 chips were then incubated in acetone (used to remove residual resist during processing) overnight, and observed by fluorescence microscopy. Again, the fluorescent signal did not change, suggesting DNA integrity is not affected by acetone solutions. The DNA-coated SiO_2 chips were then incubated at temperatures up to 150°C for 15 minutes, as would occur during photoresist curing. No change in the fluorescent signal was observed.

Although the the integrity and adhesion of DNA to SiO_2 surfaces was not adversely affected by the microfabrication chemicals and processes, DNA functionalization of the microcantilevers failed because the native oxide on the pSi was insufficient for direct adhesion of sensor biomolecules. Attempts to grow SiO_2 on the cantilevers introduced stresses that caused beam deflection and stiction that destroyed their viability. Thus, the process was modified for thiol-based biomolecular adhesion to gold surfaces, which were patterned on the cantilevers using the functionalization mask, prior to formation of the microchannels. Sample gold-patterned microcantilevers are shown in Fig. 7 after releasing from the photoresist and drying in $SCCO_2$. With the gold template in place, the microchannels are fabricated, and selective functionalization within the channels is guided by thiol chemistry with the gold surfaces. This is a simpler approach than direct adhesion to the pSi cantilevers, and eliminates microchannel processing restrictions imposed by the need to protect biomolecular layers during channel formation. There are advantages, however, to direct functionalization of the cantilevers, as discussed above, but more research will be required to develop the surface chemistry for that process to be successful.

3.1.3 Trilayer film channels

Two vital aspects of any MEMS sensor system are its mechanical robustness and its resistance to chemical attack by the solutions that will be passed through the channels. Both these issues have been addressed by Sandia's patented microchannel fabrication method, which uses a room-temperature high-density plasma to deposit a SiO_xN_y cap on channels that have been photolithographically defined using a post-processed photoresist. A scanning electron microscope (SEM) image of a sample channel is provided in Fig. 8. While SiO_2 displays excellent chemical resistance, it is rather brittle and can fracture easily. SiO_xN_y is more mechanically compliant, but it is subject to more facile chemical attack. The chemical advantages of SiO_2 and the mechanical advantages of SiO_xN_y have been combined in a trilayer film with SiO_2 surface top and bottom layers sandwiching a thin SiO_xN_y layer with a total thickness of 2 μm.

To form the microchannels, photoresist is patterned, and reflowed followed by deposition of a trilayer SiO/SiON/SiO film, and a final release of the photoresist. Important process details to successfully form robust microchannels using this technique were developed in this project. Two important findings were: (i) The aspect ratio of the resist pattern before reflowing the resist must be about 1:4 (height to width) to avoid pinch-off of the SiO/SiON/SiO film at the inside corners during film growth (Figs. 9). Microchannels on unpatterned silicon wafers that had film pinch-off discontinuity, held off pressures of only 10 psig in comparison with wider channels with oblique angles that held off pressures greater than 180 psig. (At 180 psig the interconnect failed.) (ii) The patterned resist must be post-baked to remove

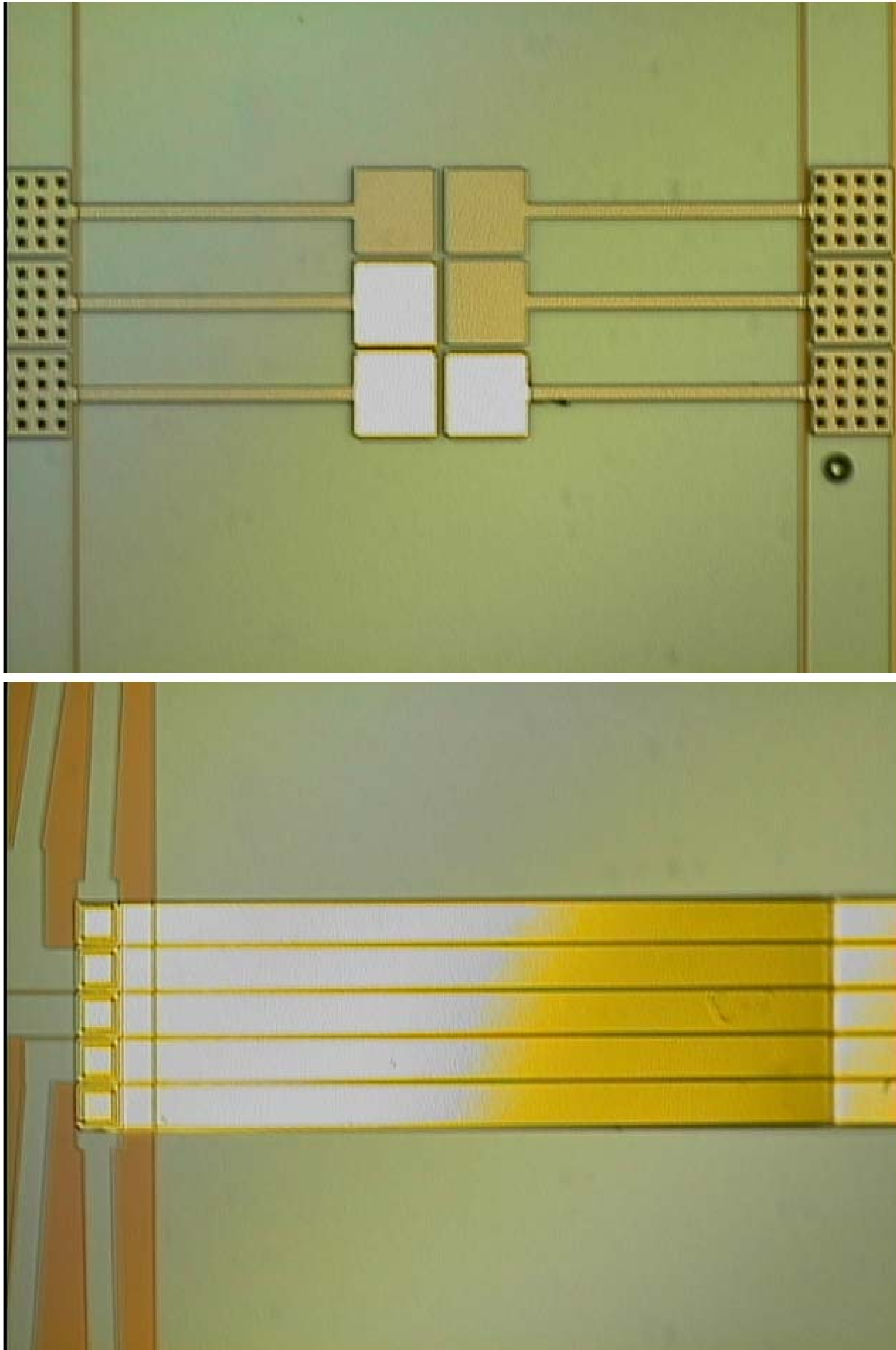

Figure 7: Photomicrographs of sample gold-patterned microcantilevers. In the upper photo, three pads are coated with gold (bright spots), and in the lower photo, the cantilevers are completely coated.

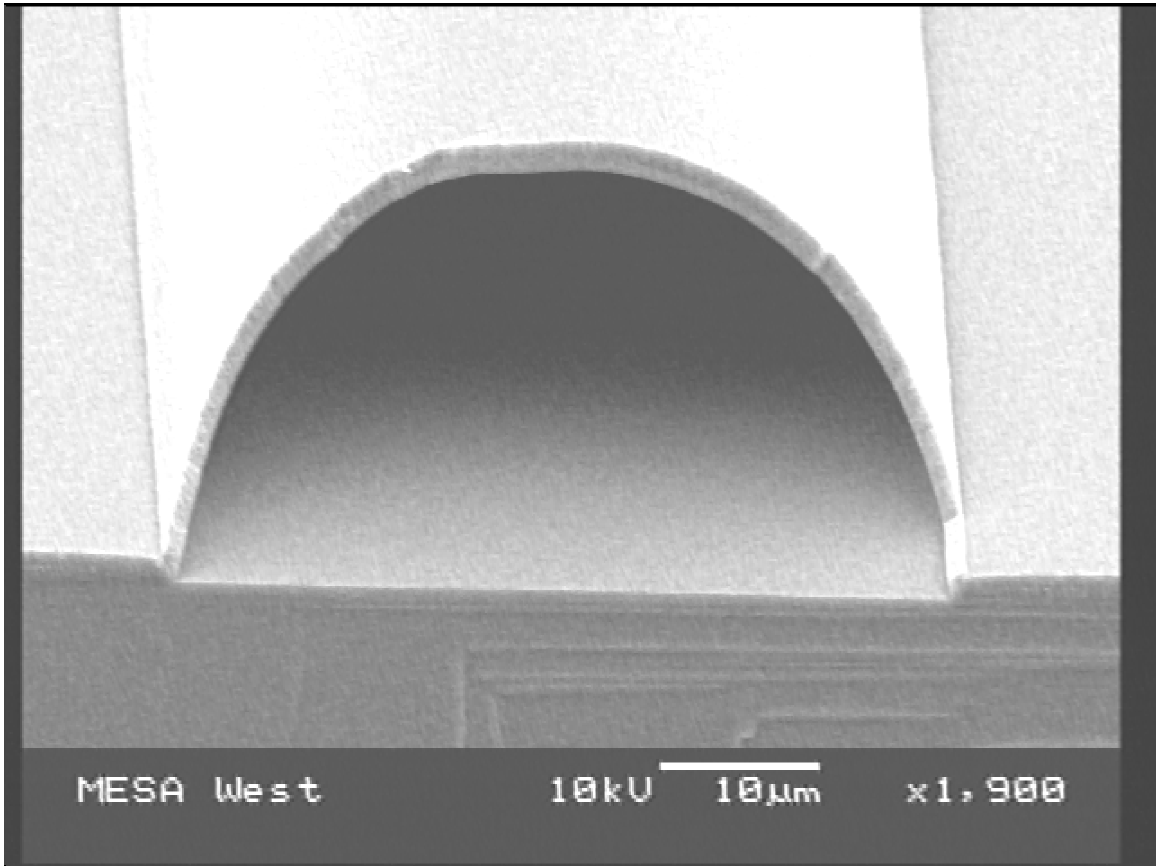

Figure 8: Scanning electron micrograph of trilayer SiO_xN_y film channel.

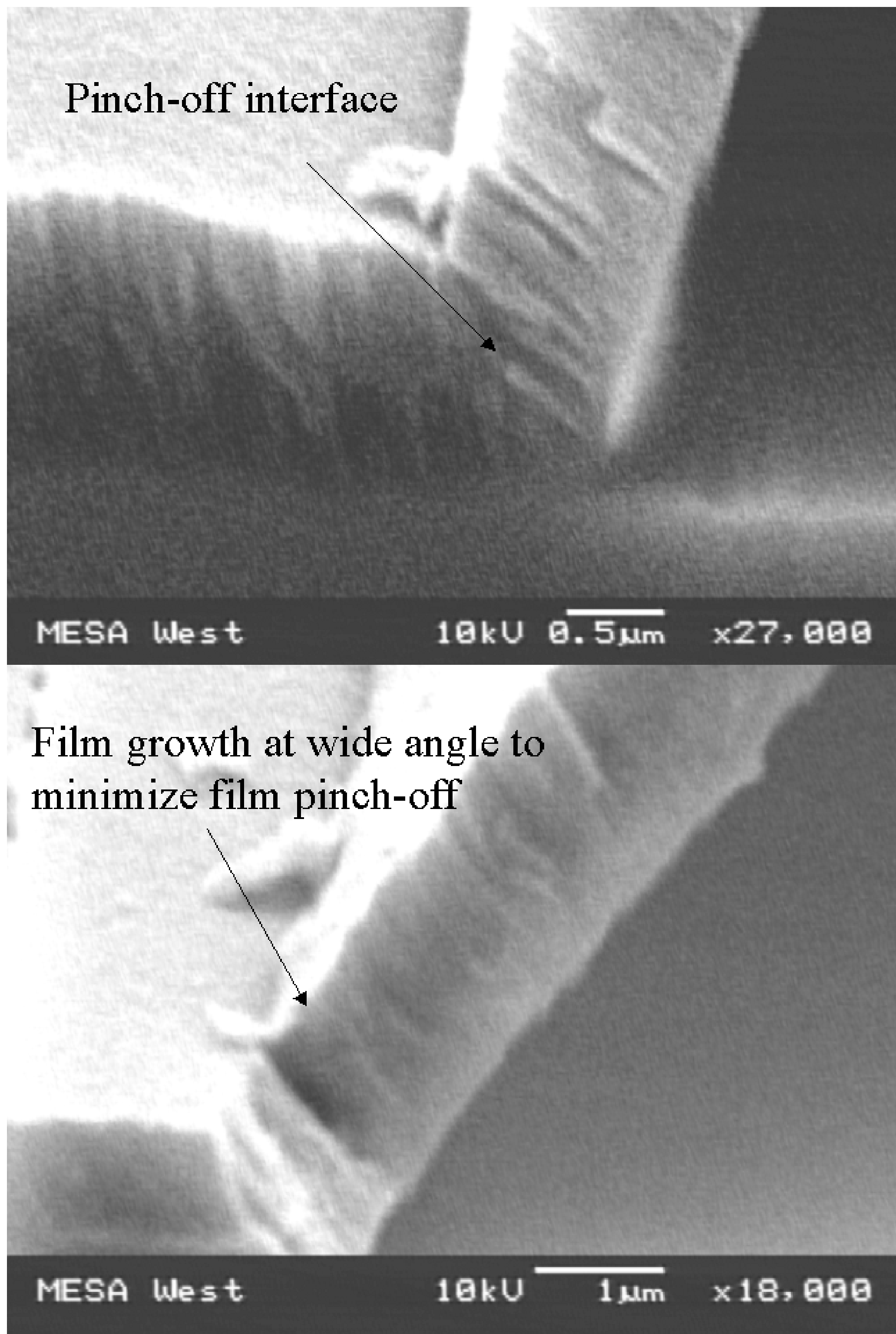

Figure 9: Scanning electron micrograph of trilayer film with and without pinch-off.

photosensitive components that react adversely with radiation in the plasma during film growth. Photoresist that was inadequately baked reacted with plasma to form cone-shaped defects that were identified by Raman as crystalline silicon material in the trilayer film (Fig. 10). For AZ5740 photoresist a post bake at 150°C remove photosensitive components. The channel height at the peak is 25 μm and the width at the base is 180 μm. This channel

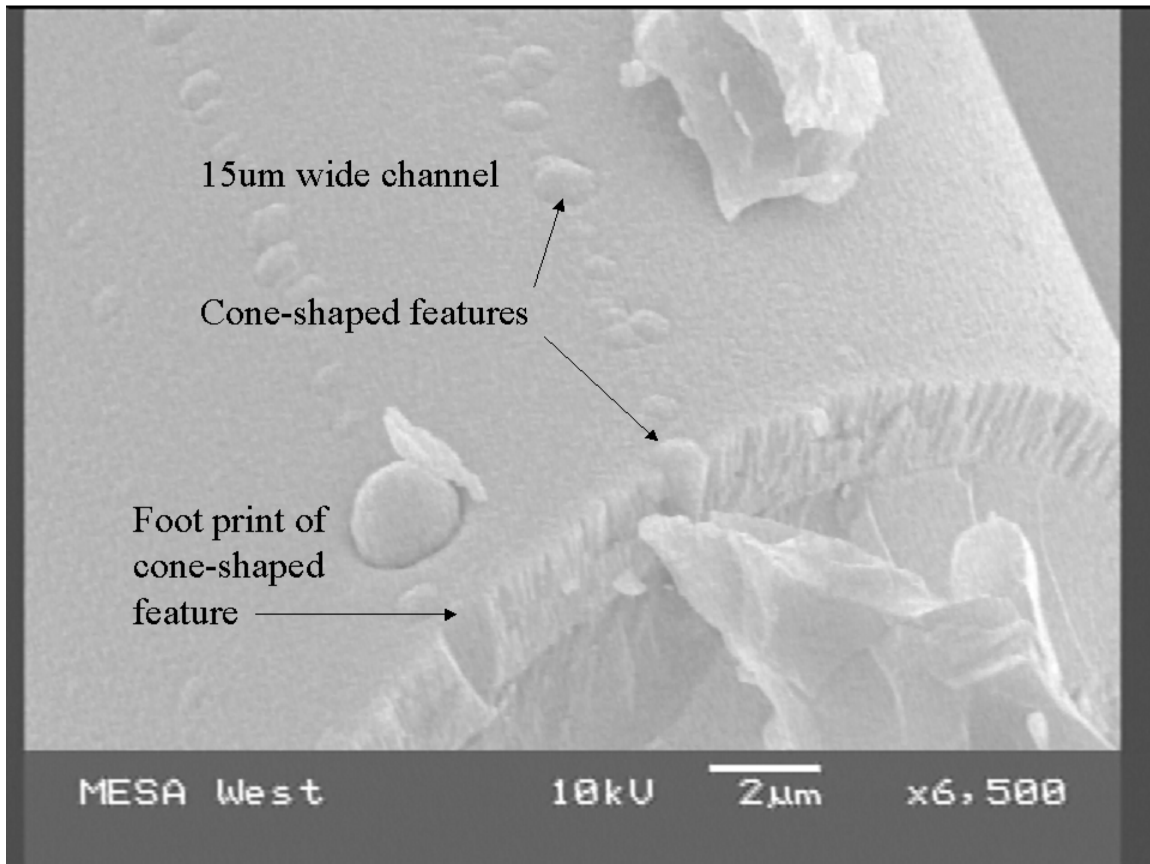

Figure 10: Scanning electron micrograph of cone-shaped defects from insufficient post-bake of photoresist.

fabrication technique is ideally suited to this application because the trilayer film can be deposited over micron-scale topography as required for electrical connections, and because processing temperatures are low enough ($\leq$ 150°C) not to destroy many biomolecular sensor coatings.

3.1.4 Releasing and drying

The fabrication process summarized in Fig. 1 requires that the MEMS devices be released and dried three times to produce chemical sensors integrated in microfluidic channels. They are first released from the sacrificial oxide layers in HF:HCl, followed by several cleaning steps, and dried in $SCCO_2$ at MDL. After patterning gold at CSRL, the cantilevers are released from photoresist in acetone and dried again in $SCCO_2$. Then after the trilayer film microchannels

are deposited on the patterned photoresist, the instrumented microfluidic chips are again released in acetone and dried in $SCCO_2$ before installation of fluid interconnects. Cantilever inspections using interferometry after each step in the fabrication process have revealed no stiction or other problems except in the final drying step. Initial attempts to dry the microfluidic chips in $SCCO_2$ fractured the channels. We hypothesized that this was caused by a differential pressure across the microchannel wall during the standard pressurization process. The pressure gradient might be caused by flow in the channel as a result of an air bubble or some other mechanical capacitance delaying the time required to propogate the applied pressure to the inside of the channels. The problem was solved by reprogramming the $SCCO_2$ drying process to ramp up the pressure more slowly (30–60 min.).

A remaining problem with the final drying step is stiction. Most cantilevers stick to the substrate after the final drying; only cantilevers $\leq$ 200 μm long remain free. These are not sensitive enough to measure flow (cf. §2.2), and have a chemical sensitivity much lower than what has been demonstrated in the literature. The problem with the last drying step is that the microcantilevers are enclosed in microchannels that are at least 2 cm long. Typical $SCCO_2$ drying schedules allow tens of minutes to a several hours for $SCCO_2$ flushing to ensure complete removal of methanol (the solvent in which wafers are submerged upon entering the drier). The schedule used for our final cantilever drying included 6 hrs of $SCCO_2$ flushing, but this was still insufficient because mixing in the microchannels occurs only by diffusion. The characteristic time t_c for diffusion across a given length l is given by

$$t_c \sim \frac{l^2}{4D}, \tag{7}$$

where D is the solutal diffusivity. For CO_2 in MeOH, $D \sim 10^{-5}$ cm^2/s, so the characteristic time for diffusion to the center of a 2 cm channel is about 7 hrs. This is only an estimate of the time required for the $SCCO_2$ to reach the center of the channel. The time required for diffusive transport to completely eliminate MeOH from the channel will be much greater, and may require days of $SCCO_2$ flushing. New procedures for $SCCO_2$ drying need to be developed for releasing MEMS structures in microfluidic channels.

3.1.5 Interconnects

The final step in the fabrication process is the installation of fluidic interconnections to off-chip pumping sources. An interconnection method was developed [30] that aligns a capillary parallel to the exposed channel end and seals the joint with a PDMS o-ring (Fig. 11). The basic installation procedure is as follows:

(1) Capillary tube (with polyimide coating removed) is aligned with the end of a channel on the MEMS wafer.

(2) PDMS ring is dispensed using an Asymtec commercial dispensing system to form a reservoir around the end of the tube and microchannel.

(3) Glass chip is placed over the reservoir to form the top reservoir cover.

(4) After 24 hour cure, assembly is potted with 2-part epoxy for additional reinforcement.

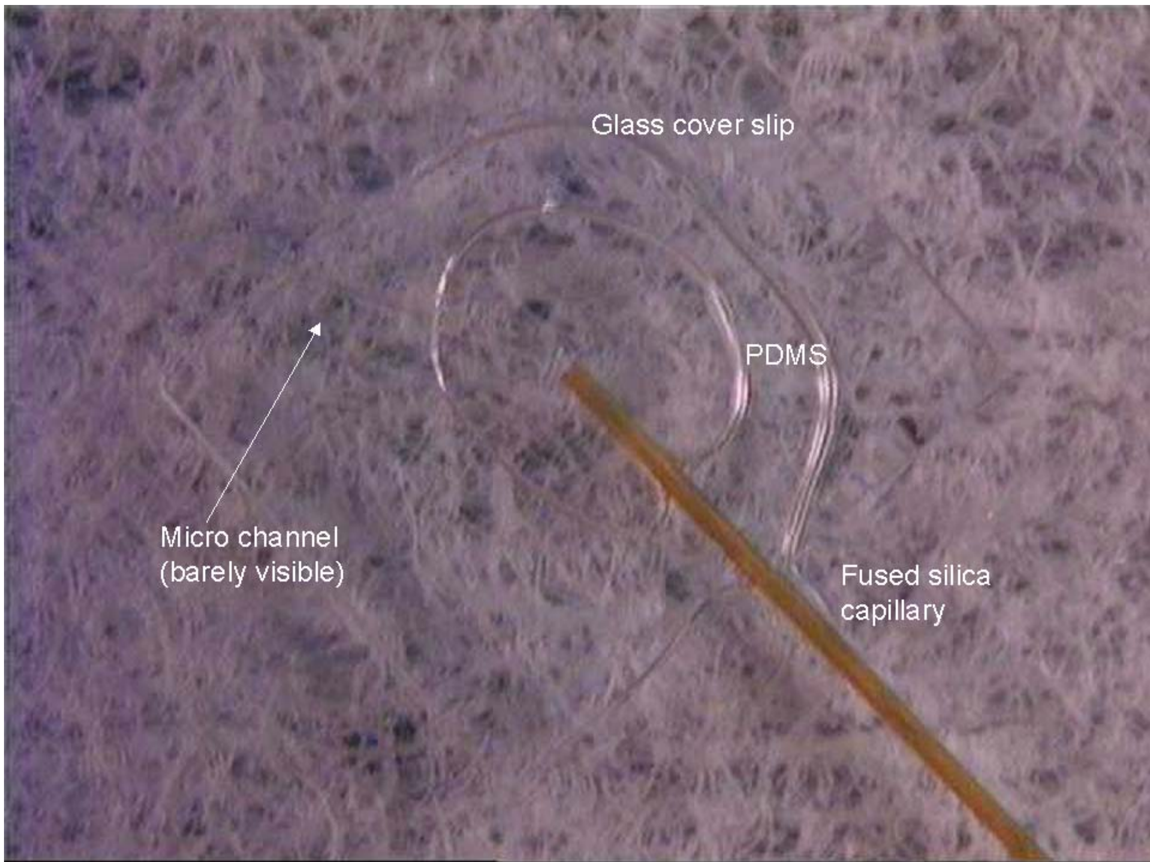

Figure 11: Photomicrograph of microfluidic channel interconnect.

3.1.6 Experimental

The second generation cantilever arrays integrated into SiO_xN_y microfluidic channels were tested at the Nanobiotechnology Center in the School of Applied and Engineering Physics at Cornell University. The channels did not leak, but reliable cantilever deflections could not be measured because of optical problems associated with the curvature of the channel surface. Cantilever deflections for these devices are on the order of nanometers, and thus require extremely sensitive out-of-plane deflection measurements. At Cornell's Nanobiotechnology Center, this sensitivity is realized with an optical system (Fig. 12) that measures the position

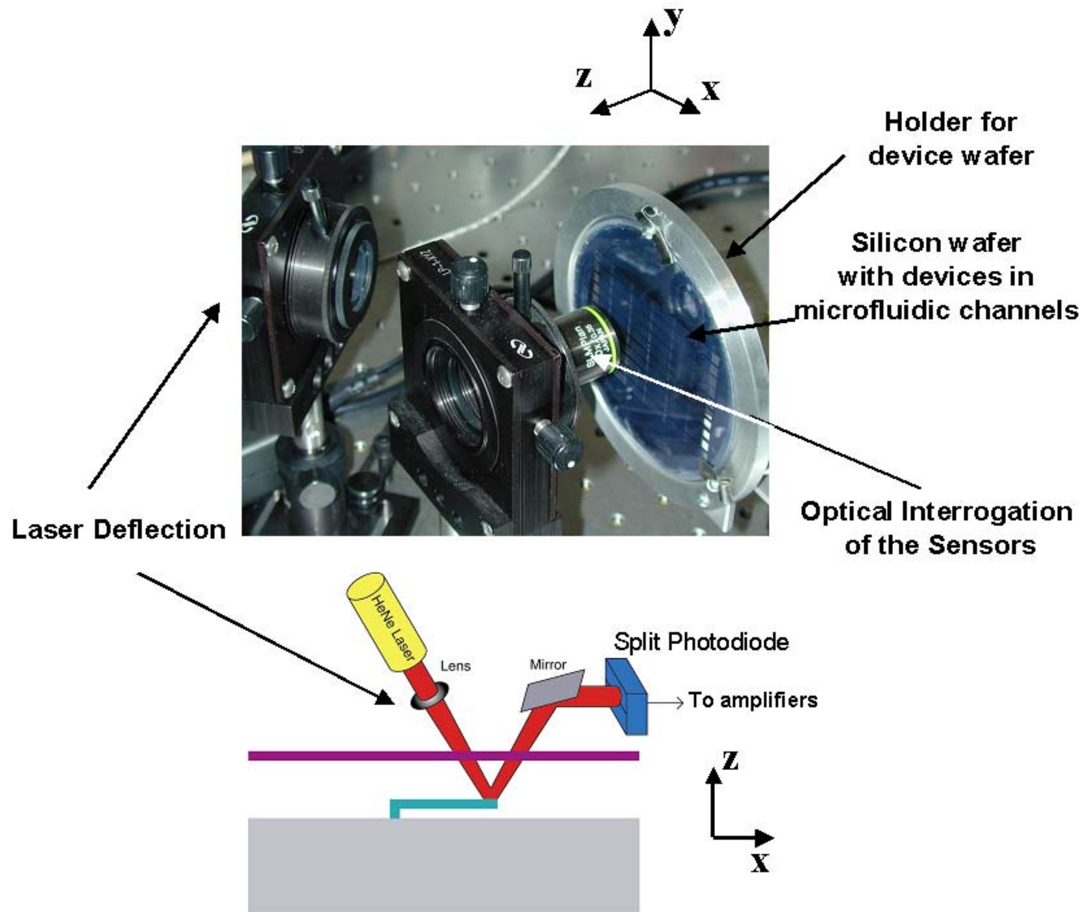

Figure 12: Schematic of the optical deflection measurement system, showing the devices on the silicon wafer mounted in the holder and the optics necessary to observe the device and focus the laser on the surface of the plate. The laser was focused onto the surface of the plate, 20 mm from the free edge of the device, the reflected laser beam was centered on a split photodiode to record the deflection of the devices. (Reproduced with permission from David Czaplewski [31].)

of a laser beam reflected off the cantilever, with a split photodiode [31, 32]. The deflection of the cantilever is magnified by the lever action of the laser. The ability to make this

sensitive measurement however is compromised by optical abberations resulting from the curved channel. Solving this problem would have required modifications to the experimental apparatus that were deemed beyond the scope of this project given that only the least sensitive cantilevers were released in the final drying step. Instead, another approach was pursued as described in the following sections.

4 Passive Cantilevers in Si/Glass Channels

The trilayer film process enables channel formation over electrical leads and temperature sensitive chemical and biological coatings, but further research is required to make the sensitive optical measurements required and to prevent stiction during drying. Flow sensing does not require active devices or functionalization, so other methods of channel formation were implemented to encapsulate flow sensors in microfluidic channels.

4.1 Cornell Wafers

Microcantilevers and other local flow sensor designs were fabricated on 4 in. Si wafers at Cornell University, and enclosed in anodically bonded microfluidic channels etched in borosilicate glass. No viable cantilevers were produced because of problems with stiction, but a derivitive design shown if Fig. 13 was tested, and successful optical detection of flow/viscosity was achieved. This work has been described in detail elsewhere [31]–[33], and will therefore only be briefly summarized here. The structure shown in Fig. 13 is oriented typically with the open end downstream, but can be used to sense fluid motion with the open end upstream also. The upper membrane deflects downward because the pressure underneath is equilibrated with the pressure at the trailing edge, but the pressure above increases towards the upstream end to balance the viscous stresses inherent in the channel flow. Flow and viscosity detection were demonstrated for several fluids including silicone oils, ethanol, and n-propanol at flow rates ranging from 2 μL/min to 40 μl/min. The sensor response is summarized in Fig. 14. The maximum sensitivity to fluid flow was determined to be 12.5 ± 0.2 μrad/(μL/min). The response at low flow rates (e.g. up to 20 μl/min for 4.6 cP silicone oil) is linear, but the sensitivity diminishes at higher flow rates. The nonlinearity occurs for Reynolds numbers $\Re \geq O(1)$, and therefore may result from inertial effects at the trailing edge of the device. The upstream influence of the trailing edge diminishes with increasing $\Re$, which reduces the differential pressure on the membrane, thus lowering the sensitivity. The significance of the edge effects is also implied by a response that differs when the open end of the device is oriented upstream. The fluid motion and sensor plate deformation were also simulated with FEM analyses, which predict a significantly lower deformation than measured, and also suggest the importance of the edge effects.

4.2 Sandia MDL Wafers

The interesting behavior observed for the flow sensors fabricated at Cornell suggests that microcantilever deflection might also deviate significantly from theory. If the measured deflections of those devices were higher than predicted because of edge effects, then the

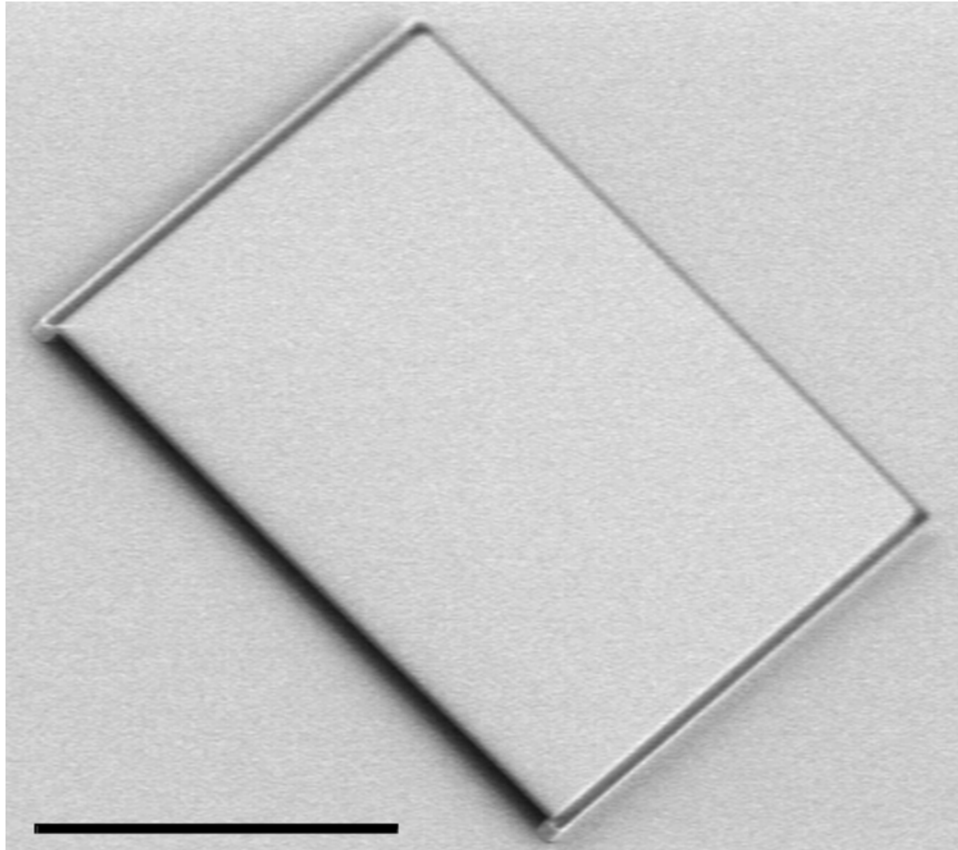

Figure 13: Scanning electron micrograph showing a tilted and rotated view of the micromechanical plate flow sensor. The top left, top right and bottom right sides of the plate are rigidly clamped to the substrate while the bottom left remains free to move. (Reproduced with permission from David Czaplewski [31].)

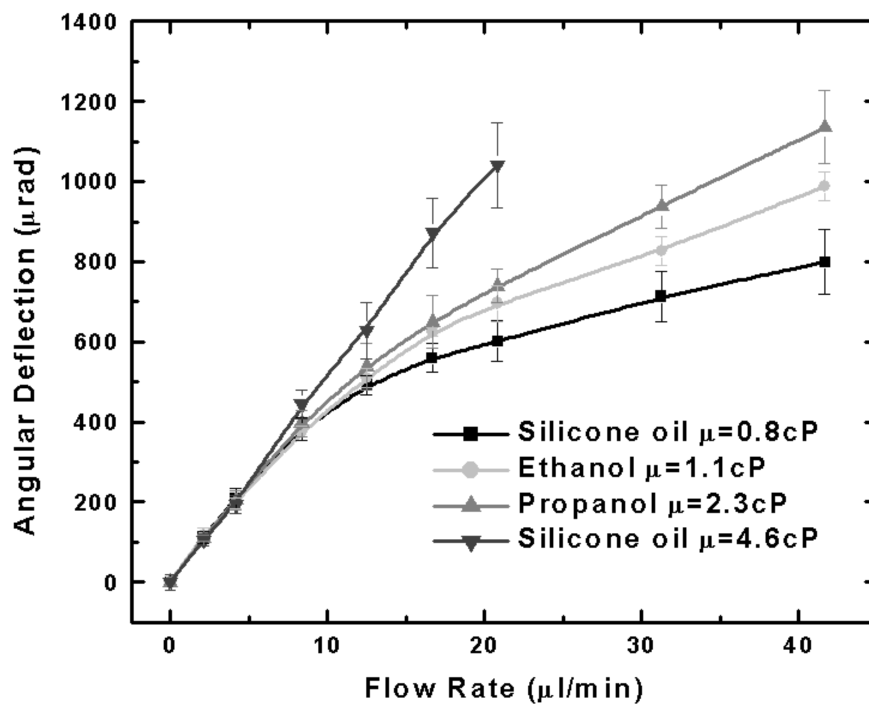

Figure 14: Response of the flow sensing micromechanical plate to various flow rates of different fluids. (Reproduced with permission from David Czaplewski [31].)

cantilever deflections should deviate even farther from theory because they are more sensitive to the flow at the trailing edge. This led us to an interest in anodically bonding Cornell's glass channels to Sandia's wafers instrumented with the cantilever arrays. This required a new approach to the fabrication process, which we have developed and are in the process of implementing. Glass channels have been etched 30 μm deep in 4 in. wafers from a mask made to match the die pattern on the MEMS wafer. The channel walls are 120 μm wide and positioned to align with the poly0 borders that separate the die, thus enabling an anodic bond to a quartered 6 in. Si MEMS wafer. One of Sandia's Si wafers has been quartered, backside via holes have been sandblasted to provide fluidic access to the channels, and the devices (including 500μm and 1 mm long cantilevers) have been successfully released and dried. The last step in the new fabrication process is the anodic bond, and when this is completed, the devices will be tested at Cornell's Nanobiotechnology Center. This process eliminates problems with drying devices in microfluidic channels, and produces MEMS in microchannels with optically flat surfaces.

5 Electrostatic Actuation in Liquids

One of the key challenges for actuated sensors embedded in liquid-filled channels is interference of the liquid with the actuation mechanism. This is particularly problematic for electrostatic actuators such as those developed at MDL because even small concentrations of ions in essentially pure liquids screen the electrode charge (electrode polarization) and disable the actuator. However, using ac drive signals, we have demonstrated electrostatic actuation in many liquids, at potentials low enough to avoid electrochemistry [34, 35]. Sensors have been successfully actuated in water, requiring a frequency of only 100 kHz for maximum displacement. We have measured the frequency response in liquids spanning a decade of dielectric permittivities and four decades of conductivity, and have developed an elegant theory that predicts the characteristic actuation frequency

$$f_{\mathrm{c}} = \frac{\sigma b}{\varepsilon_{\mathrm{ox}} \varepsilon_0 g} \tag{8}$$

for a silicon MEMS device in a sufficiently ionic medium ($\kappa_{\mathrm{eff}} b \varepsilon_{\mathrm{dl}} / \varepsilon_{\mathrm{ox}} \gg 1$), in the absence of faradaic processes; σ is the electrical conductivity, b and $\varepsilon_{\mathrm{ox}}$ are the oxide thickness and dielectric permittivity, respectively, ε_0 is the permittivity of free space, g is the thickness of the gap between the electrodes, and κ_{eff} and $\varepsilon_{\mathrm{dl}}$ are the double layer thickness and permittivity, respectively. The measured and predicted actuation frequencies are summarized in Fig. 15. The theory shows that, although only a few nanometers in thickness, the native silicon oxide layer increases the actuation frequency by more than an order of magnitude relative to that of an inert electrode, and explains a measured linear dependence of actuation frequency on conductivity. Our results show that integrated electrostatic actuation in microfluidic MEMS is feasible in electrolytes of ionic strength up to at least 10–100 mmol/L, and is therefore suitable for some biological sensing applications, but requires RF signal generators, amplifiers, and circuits. More details on this work can be found in [35].

In support of this work, two copywrighted products have been produced. A benchtop high power/high frequency amplifier was developed and fabricated to enable actuation in water at

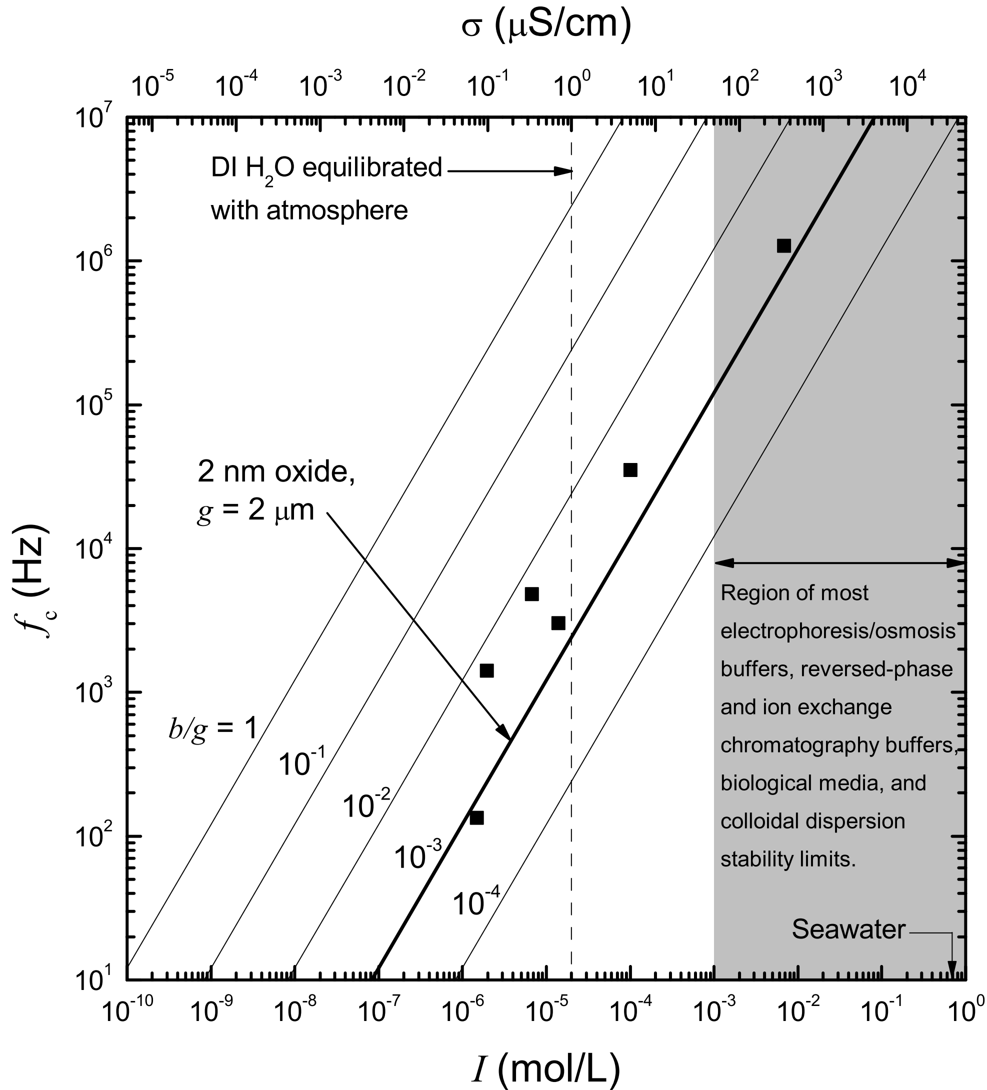

Figure 15: Critical electrostatic actuation frequency at selected values of b/g. Lines from theory if $\kappa_{\text{eff}} b \varepsilon_{\text{dl}} / \varepsilon_{\text{ox}} \ll 1$ ($\varepsilon_{\text{ox}} = 4.5$); squares from comb drive actuator response data. The conversion of conductivity to ionic strength assumes an ion mobility of sodium (5×10^{-4} cm^2/V-s), which has a typical value for ions that normally carry the current in a conducting solution.

applied potentials up to 100 V [36]. This instrument has found extensive use in and outside Sandia, and over 15 units have been built to date. Also, we have written and copywrighted software for actuating MEMS microengines that is being negotiated for licensed distribution to a MEMS development company [37].

6 Conductivity Sensor

The study of electrostatic actuation in liquids led us to invent a novel electromechanical technique for measuring electrical conductivity. Our work with electrostatic comb-drives revealed that for silicon actuators in most liquids, the actuation frequency is linear in conductivity and independent of other fluid properties (cf. Eq. (8)). In the conductivity measurement, small currents do not have to be measured, so Faraday cages are not required. Also, there are no faradaic processes at the electrodes, which simplifies the interfacial impedance and eliminates electrochemical transformations in the system. Fluid conductivities from 70 nS/cm to 200 μS/cm were measured with a silicon MEMS device, and a patent disclosure has been submitted [38].

7 Hydrodynamic Damping Reduction

Another key challenge for dynamic microfluidic sensors is liquid damping. Most microcantilevers are overdamped in water and are thus not viable resonance sensors. Cantilevers shorter than approximately 100 μm may resonate, but their sensitivies are extremely low due to a low quality factor. We explored coatings for damping reduction in MEMS based on hydrophobic slip at liquid-solid interfaces. We determined that damping reduction from hydrophobic SAM coatings is too small to significantly impact MEMS devices with micron scale gaps, but a new coating recently developed at Sandia has been demonstrated to significantly reduce drag even in macroscale systems. We began synthesis of these coatings in microscale systems and measured a 5% drag reduction in a microcapillary even though it was only poorly coated. Orders of magnitude more reduction in damping is expected when proper synthesis is accomplished in microscale devices.

8 Concluding Remarks

A new microfluidic MEMS fabrication process has been developed that encapsulates electrically addressable MEMS devices in microfluidic channels, and because of the low temperature channel formation process, embedded chemical sensors can be biomolecularly functionalized before or after channel formation using gold templates. Several microcantilever-based sensor designs have been produced to detect fluid motion and biomolecules, and integrated into microfluidic architectures with robust interconnections to off-chip pressure sources. In-situ local flow measurements have been demonstrated, and research on sensor performance continues. Releasing MEMS devices that have been wetted in microfluidic channels requires modification of standard $SCCO_2$ drying schedules, which are designed to flush methanol out

of microscale features on open wafers. Binary diffusion calculations and experimental verification are needed to generate new standard drying procedures for microfluidic channels, with the channel length as a key parameter. Electrostatic actuation has also been demonstrated in several liquids including water, and an elegant theory has been developed that defines the requirements quantitively with a simple equation. This work also has led to the development of a novel microscale method of measuring conductivity that is particularly important for low conductivity fluids. The work in this project has resulted in several conference presentations, four published papers, two copywrights, one patent, and one patent disclosure.

References

[1] J.W. Judy, *Smart Mater. Struct.* **10**, 1115–1134 (2001).

[2] http://www.mems.sandia.gov

[3] C.M. Matzke, C.H. Ashby, M.M. Bridges, R.P. Manginell, U.S. Patent 6,096,656, Aug. 1, 2000.

[4] H.P. Lang, M.K. Baller, R. Berger, Ch. Gerber, J.K. Gimzewski, F.M. Battiston, P. Fornaro, J.P. Ramseyer, E. Meyer, H.J. G untherodt, *Analytica Chimica Acta* **393**, 59–65 (1999).

[5] A.M. Moulin, S.J. O'Shea, M.E. Welland, *Ultramicroscopy* **82**, 23–31 (2000).

[6] J. Fritz, M.K. Baller, H.P. Lang, H. Roghuizen, P. Vettiger, E. Meyer, H.J. G untherodt, Ch. Gerber, J.K. Gimzewski, *Science* **288**, 316–318 (2000).

[7] G. Wu, H. Ji, K. Hansen, T. Thundat, R. Datar, R. Cote, M.F. Hagan, A.K. Chakraborty, A. Majumdar, *Proc. Natl. Acad. Sci.* **98**, 1560–1564 (2001).

[8] G. Wu, R.H. Datar, K.M. Hansen, T. Thundat, R.J. Cote, A. Majumdar, *Nature Biotechnology* **19**, 856–860 (2001).

[9] K.M. Hansen, H. Ji, G. Wu, R.H. Datar, R.J. Cote, A. Majumdar, T. Thundat, *Anal. Chem.* **73**, 1567–1571 (2001).

[10] J. Tamayo, A.D.L. Humphris, A.M. Malloy, M.J. Miles, *Ultramicroscopy* **86**, 167–173 (2001).

[11] B. Ilic, D. Czaplewski, M. Zalalutdinov, H.G. Craighead, P. Neuzil, C. Campagnolo, C. Batt *J. Vac. Sci. Technol. B* **19**, 2825–2828 (2001).

[12] M. Su, S. Li, V.P. Dravid, *Appl. Phys. Lett.* **82**, 3562–3564 (2002).

[13] M. Royer, P. Holmen, M. Wurm, P. Aadland, M. Glenn, *Sens. Actuators A* **4**, 357–362 (1983).

[14] L. Löfdahl and M. Gad-el-Hak, *Meas. Sci. Technol.* **10**, 665–686 (1999).

[15] M. Schmidt, R. Howe, S. Senturia, J. Haritonidis, *IEEE Trans. Electron. Dev.* **35**, 750–757 (1988).

[16] A. Padmanabhan, H. Goldberg, K.D. Breuer, M.A. Schmidt, *J. MEMS* **5**, 307–315 (1996).

[17] S.T. Cho and K.D. Wise, *Sens. Actuators A* **36**, 47–56 (1993).

[18] N.T. Nguyen, *Flow Meas. Instrum.* **8**, 7–16 (1997).

[19] A. Rasmussen and M.E. Zaghloul, *Circuits & Devices* **14**, 12–21 (1998).

[20] A.F.P. Van Putten, S. Midelhoek, *Electronic Letters* **10**, 425–426 (1974).

[21] J. Tanaka, A. Jinda, H. Tabuchi, N. Tanaka, H. Furubayashi, Y. Inami, M. Hijikigawa, *Proc. of the 6th Sensor Symposium*, The Institute of Electrical Engineers of Japan, Japan, 1986, pp. 125–129.

[22] R.G. Johnson and R.E. Egashi, *Sens. Actuators A*, **11**, 63–67 (1987).

[23] M. Esashi, *Sens. Actuators A* **21**, 161–167 (1990).

[24] C.Q. Yang and H. Soeberg, *Sens. Actuators A* **33**, 143–153 (1992).

[25] T.S.J. Lammerink, N.R. Tas, M. Elwenspoek, J.H.J. Fluitman, *Sens. Actuators A*, **37-8**, 45–50 (1993).

[26] N.T. Nguyen, A.H. Meng, J. Black, R.M. White, *Sens. Actuators A* **79**, 115–121 (2000).

[27] A. Rasmussen, C. Mavriplis, M.E. Zaghloul, O. Mikulchenko, K. Mayaram, *Sens. Actuators A* **88**, 121–132 (2001).

[28] C. Liu, J.-B. Huang, Z. Zhu, F. Jiang, S. Tung, Y.-C. Tai, C.-M. Ho, *J. MEMS* **8**, 90–99 (1999).

[29] S.G. Joshi, *Sens. Actuators A*, **44**, 63–72 (1994).

[30] C.M. Matzke, C.H. Ashby, L. Griego, U.S. Patent 6,599,436 B1, Jul. 29, 2003

[31] D.A. Czaplewski, "Micromechanical and Microfluidic Devices, Their Fabrication, Operation, and Application," Ph.D. Dissertation, Cornell University, 2004.

[32] D.A. Czaplewski, B. Ilic, M. Zalalutdinov, W.L. Olbricht, A.T. Zehnder, H.G. Craighead, T.A. Michalske, accepted to *Journal of Microelectromechanical Systems*, 2004.

[33] D.A. Czaplewski, B. Ilic, M. Zalalutdinov, W.L. Olbricht, A.T. Zehnder, H.G. Craighead, T.A. Michalske, *Transducers '03*, Boston, MA, June 8–12, 2003, 392–395.

[34] T.L. Sounart, T.A. Michalske, *Transducers '03*, Boston, MA, June 8–12, 2003, 615–618.

[35] T.L. Sounart, T.A. Michalske, K.R. Zavadil, submitted to *Journal of Microelectromechanical Systems.*

[36] K.R. Pohl, M.W. Jenkins, T.L. Sounart, Sandia Copywright Number (SCR) 702, Dec. 22, 2003.

[37] M.W. Jenkins, T.L. Sounart, Export Control Classification Number (EECN) EAR99, Jan. 24, 2003.

[38] TA #SD-7624

DISTRIBUTION:

1	MS 0161	C.L. Ashby, 11500
1	0323	D.L. Chavez, 1011
1	1080	M. Okandan, 1749
5	1411	T.L. Sounart, 1846
1	1413	T.A. Michalske, 1040
1	1413	C.M. Matzke, 1141

1	MS 9018	Central Technical Files, 8945-1
2	0899	Technical Library, 9616
1	0161	Patent and Licensing Office, 11500